A Compact Dual-Band Single-Feed Slotted Waveguide Array Antenna for Unidirectional Radiation Patterns

Aritra Roy, Rozenn Allanic, Thierry Le Gouguec, François Gallée, Erwan Fourn, Anne-Charlotte Amiaud, Hervé Legay

A Compact Dual-Band Single-Feed Slotted Waveguide Array Antenna for Unidirectional Radiation Patterns

Aritra Roy, *Member, IEEE,* Rozenn Allanic, *Member, IEEE,* Thierry Le Gouguec, *Member, IEEE,* Francois Gallee, *Member, IEEE,* Erwan Fourn, *Member, IEEE,* Anne-Charlotte Amiaud, Hervé Legay,

***Abstract*—A dual-band slotted waveguide array (SWA) antenna is designed using a single waveguide by placing the radiating slots for 18 GHz and 24 GHz on the same antenna aperture. These bands are excited using a single excitation point through a conventional waveguide feeding technique to radiate unidirectional radiation patterns of same polarization. Theoretical analyses are carried out to study the conductance of the slots to understand their effects on the dual-band performance. Numerical analyses are performed to optimize the antenna by considering mutual coupling. The antenna is fabricated using stereolithography (SLA) and direct metal laser sintering (DMLS) processes to compare its performance in different additive manufacturing techniques. In characterizing the fabricated prototype, an impedance matching of $|S_{11}| < -10$ dB and the boresight antenna gains of 14 dBi and 17.4 dBi are measured in these bands with unidirectional and linearly polarized radiation patterns. A quantitative comparison among dual-band SWA antennas is presented at the end of the manuscript to highlight the uniqueness of the proposed approach over the state-of-the-art solutions.**

***Index Terms*—Antenna, dual-band, slot-array, waveguide**

I. Introduction

A slotted waveguide array (SWA) antenna widely used for defence, space and telecommunication applications is known for its high power handling capability due to the robust all-metal structure, offers a high gain and unidirectional radiation pattern [1]. Its narrow beams in conjunction with power division networks can be utilised for beam scanning in low-earth orbit (LEO) constellation satellite systems or in direction-finding in radars and MIMO systems [2]. These antennas are designed by engraving narrow slots on the walls of a waveguide to guide the slot radiation in the far field constructively. The theoretical characteristics of a slot on the broad wall of a waveguide by Stevenson [3] inspired the design of a boresight radiator by Elliot [1], [4], [5], and was experimentally verified by Stegan [6], [7]. The slot length and periodicity are determined from the resonance frequency which inherently restricts the antenna operation at a single frequency and limits its usage for dual or multi-band applications.

A dual-band solution with SWA antennas was presented by introducing longitudinal and lateral slots in the broad and narrow walls of successive waveguides fed through multiple irises in the feeding network [8]. This technique uses a complicated feeding geometry and sacrifices the compactness of the antenna while radiating two polarisations at two frequencies. A similar structure with a simplified feed was reported with an identical polarisation response in [9]. An efficient design technique is adapted to radiate uni-polarized waves at different frequencies by accurately aligning two radiating layers that are excited through a single excitation point [10]. However, it was implemented using substrate-integrated waveguide (SIW) technology which limited the power handling capacity of the antenna. Another single-feed dual-band SWA was designed by placing slots on both broad walls of the waveguide to radiate two polarisations through bidirectional radiation patterns [11]. This geometry is slightly modified for single polarisation by adjusting the slot placement but with a bidirectional radiation pattern [12]. A solution for unidirectional radiation is presented with two waveguides for different frequencies with an electrically large structure in [13]. An efficient dual-band SWA was earlier reported by our group where two waveguides of different cut-off frequencies are cascaded to produce unidirectional radiation patterns while retaining the polarisation in both bands [14], [15]. Despite the simplicity of this geometry, this antenna is bulky and may have high side lobes, especially at higher frequencies.

This work was supported by Thales.

A. Roy is with Lab-STICC, Universite de Bretagne Occidentale, 29200 Brest, France (e-mail: roy.aritra92@ieee.org).

R. Allanic is with Lab-STICC, Universite de Bretagne Occidentale, 29200 Brest, France (e-mail: rozenn.allanic@univ-brest.fr).

T. Le Gouguec is with Lab-STICC, Universite de Bretagne Occidentale, 29200 Brest, France (e-mail: thierry.legouguec@univ-brest.fr).

F. Gallee is with Lab-STICC - IMT Atlantique, 29280 Plouzane, France (e-mail: francois.gallee@imt-atlantique.fr).

E. Fourn is with University of Rennes, INSA Rennes, CNRS IETR-UMR CNRS 6164, F-35000, Rennes, France (e-mail: Erwan.Fourn@insa-rennes.fr).

A-C. Amiaud is with Thales LAS, 78990 Elancourt, France (e-mail: anne-charlotte.amiaud@thalesgroup.com).

H. Legay is with Thales Alenia Space, 31100 Toulouse France (e-mail: herve.legay@thalesaleniaspace.com).

Corresponding author: *A. Roy*

This article has been accepted for publication in IEEE Transactions on Antennas and Propagation. This is the author's version which has not been fully edited and content may change prior to final publication. Citation information: DOI 10.1109/TAP.2024.3484150

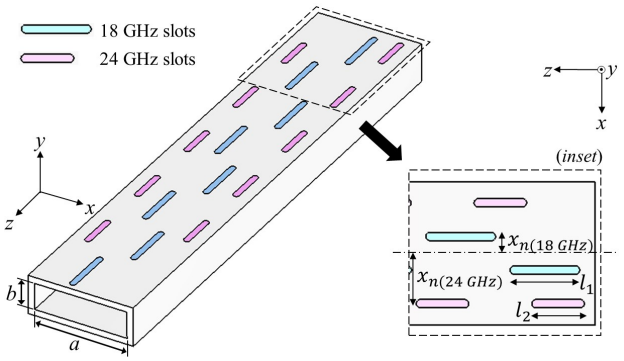

Fig. 1. Schematic of the proposed dual-band SWA antenna

This work presents a compact dual-band SWA antenna design by placing the radiating slots for the two operating bands on the broad wall of a single waveguide. Unidirectional radiation patterns are generated with the same polarization at both frequencies using a conventional waveguide excitation. Circuit-based and numerical analyses are carried out to explain the working of the proposed antenna. Fabrication with two different additive manufacturing techniques is demonstrated and their comparative responses and limitations are explained with measured results [16]. The manuscript is arranged in the following sections: the circuit model and numerical analyses are discussed in Sec.II, the fabrication and measurement in Sec. III, and conclusion in Sec. IV.

II. Analysis of the Proposed Dual-Band Antenna

A. Schematic

A schematic of the proposed dual-band SWA antenna is shown in Fig. 1. The antenna consists of a rectangular waveguide of a = 15 mm and b = 4.318 mm and two sets of 8 and 10 longitudinal slots for the operating bands of 18 GHz and 24 GHz, respectively. Each set of slots is arranged in tandem with the antenna axis. Theoretically, each slot must have a length of $\lambda_0/2$, where λ_0 is the free space wavelength of the operating frequency, which can be slightly adjusted to optimise the overall antenna response. In the proposed structure, lengths l_1 = 8.3 mm and l_2 = 6.3 mm are obtained to ensure the radiation at 18 GHz and 24 GHz, respectively. The slots have a periodicity of $\lambda_g/2$ while the one near the close end of the waveguide is $\lambda_g/4$ away from it (λ_g is the guided wavelength). The slot configuration is maintained to appropriately cut the waveguide current to maximise the radiation from the antenna. The tandem arrangement is implemented by laterally moving the slots away from the antenna axis by $x_{n(18GHz)}$ and $x_{n(24GHz)}$ for 18 GHz and 24 GHz as shown in the Fig. 1(*inset*). These offset values deciding the antenna input impedance and the excitation coefficients of the slot array can be exploited to design the radiator's H-plane ($y-z$) radiation pattern. The slot width and thickness of the waveguide wall are maintained at 1 mm to comply with the fabrication design rules. The proposed antenna incorporates the radiating slots on the same aperture of the antenna to ensure unidirectional radiations in both frequencies which is unlike any reported works in literature. The following section explains the dual-band operation of the proposed arrangement using the circuit model and numerical analysis.

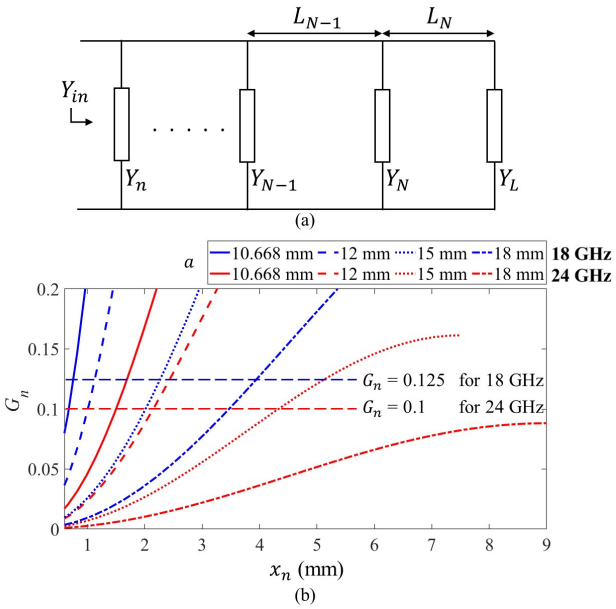

Fig. 2. (a) Equivalent circuit model of a longitudinal slot-loaded waveguide, (b) Normalized slot conductance G_n against slot offset x_n, at 18 GHz and 24 GHz considering different values of a

B. Circuit Model Analysis

The circuit model of longitudinal slots on the waveguide broadwall is shown in Fig 2(a). This model is widely used to design SWA antennas accurately while neglecting the mutual coupling between the slots. The longitudinal slots are modelled as normalised shunt-admittances $Y_n = G_n + jB_n$, where, G_n and B_n are the normalised shunt conductance and susceptance of the n-th slot. Since the waveguide is terminated with a metallic wall (short circuit) as in a SWA geometry, the value of load impedance Y_L can be assumed to be infinitely high. N being the total number of longitudinal slots, the N-th slot is placed at a distance of L_n = λ_g/4 away from the load while their periodicity is maintained at L_n = λ_g/2, n = 1, 2, ..., N-1. The slots resonate at the operating frequency and offer real-valued admittances with B_n = 0. Therefore, the normalised input admittance of the slot-loaded waveguide can be calculated at the resonant frequency as [6]

$$Y_{in} = \sum_{n=1}^{N} Y_n = \sum_{n=1}^{N} G_n \tag{1}$$

This article has been accepted for publication in IEEE Transactions on Antennas and Propagation. This is the author's version which has not been fully edited and content may change prior to final publication. Citation information: DOI 10.1109/TAP.2024.3484150

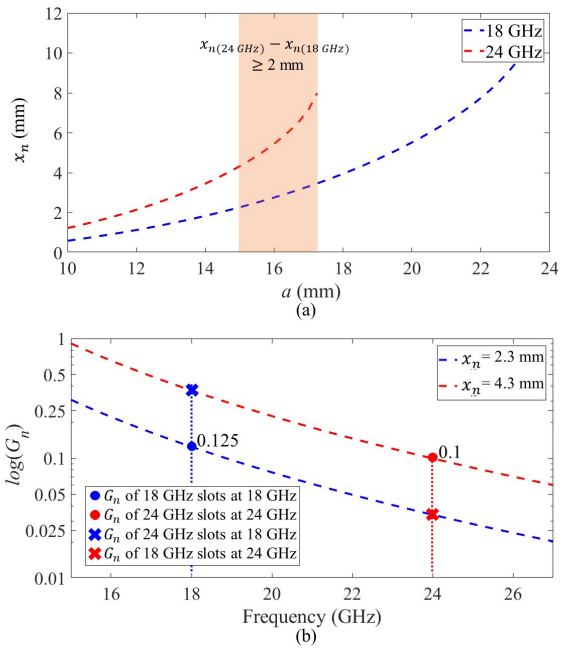

Fig. 3. (a) Slot offset x_n for different values of waveguide width a, (b) Normalized slot conductance G_n as a function of frequency for different values of x_n

Now, since the radiated power from a slot is proportional to the square of the voltage amplitude across the slot, G_n can be expressed as a function of the excitation coefficient of the corresponding slot as

$$G_n = Ka_n^2 \tag{2}$$

where, a_n is the excitation coefficient of the nth slot and K is a proportionality constant. Now, considering an input matching at the operating frequency, Eq.(1) can be rearranged as

$$Y_{in} = \sum_{n=1}^{N} Ka_n^2 = 1 \tag{3}$$

and Eq. (2) can be written as

$$G_n = \frac{a_n^2}{\sum_{n=1}^{N} a_n^2} \tag{4}$$

Now, the normalized slot conductance of a resonant longitudinal slot on a rectangular waveguide can be expressed as a function of the antenna dimensions as

$$G_n = 2.09\frac{a}{b}\frac{\lambda_g}{\lambda_0}cos^2(\frac{\pi}{2}\frac{\lambda_0}{\lambda_g})sin^2(\frac{\pi x_n}{a}) \tag{5}$$

where, a and b are the cross-sectional dimensions of the waveguide, λ_0 and λ_g are the free space and guided wavelengths and x_n is the lateral slot offset from the waveguide axis. This key equation of SWA antenna design in conjunction with Eq.(1) can be used to determine the impedance and radiation performance of the antenna in terms of its geometric parameters.

The farfield ($f(\theta)$) of a slot is proportional to that of a $\lambda_0/2$ radiator as

$$f(\theta) = \frac{cos(\frac{\pi}{2}cos\theta)}{sin\theta} \tag{6}$$

Hence, the overall antenna radiation ($E(\theta)$) from the slot array can be expressed as

$$E(\theta) = f(\theta)\sum_{n=1}^{N} a_n e^{jnk\frac{\lambda_g}{2}cos\theta} \tag{7}$$

where, $k = \frac{2\pi}{\lambda_0}$ and θ is the angle of observation in the H-plane.

We aim to develop a K-band SWA antenna for 18 GHz and 24 GHz by placing the resonant slots on the same broadwall of a waveguide. The normalised slot conductance G_n from Eq.(4) can be calculated as 0.125 and 0.1 for 8 and 10 slots at these frequencies, assuming a uniform array excitation (a_n = 1). The same is plotted from Eq.(5) against x_n for different values of a as shown in Fig. 2(b). It can be observed that the slots for the higher band ($x_{n(24\ GHz)}$) are placed away from the antenna axis compared to those of the lower band ($x_{n(18\ GHz)}$), which may help in placing them without an overlap. Overlapping of slots may significantly affect the overall antenna response which cannot be estimated by Elliot's law designed for a single frequency of operation. A commercial WR - 42 (10.668 mm×4.318 mm) waveguide usually employed for this frequency range offers small x_n values at 18 GHz and 24 GHz and may have overlapped slots. Moreover, it violates the fabrication design rule of a minimum inter-slot distance of 2 mm ($x_{n(24\ GHz)} - x_{n(18\ GHz)}$), hence abandons its usage for a dual-band design. The design rule is according to the resolution of the fabrication technique which must be obeyed to ensure sufficient overall performance despite the fabrication errors. This issue may be overcome by increasing the waveguide width, where the desired G_ns can be achieved with higher x_ns and the inter-slot distance can be increased. It can also be observed that the conductance varies slowly against a at the higher band which reduces the variation of input impedance with x_n as will be discussed in the following section. The x_n are plotted at the two operating bands in Fig. 3(a) to determine the optimum value of a [17]. A width between 15 mm and 17.5 mm offers a feasible design of a SWA antenna by adhering to the design rule as indicated by the highlighted zone in the figure. Since higher values of a may degrade the side lobe performance of the antenna and its array in E-plane, a = 15 mm is considered in our design as an optimum dimension and $x_{n(18\ GHz)}$ = 2.3 mm and $x_{n(24\ GHz)}$ = 4.3 mm are calculated using Eq.(5).

This article has been accepted for publication in IEEE Transactions on Antennas and Propagation. This is the author's version which has not been fully edited and content may change prior to final publication. Citation information: DOI 10.1109/TAP.2024.3484150

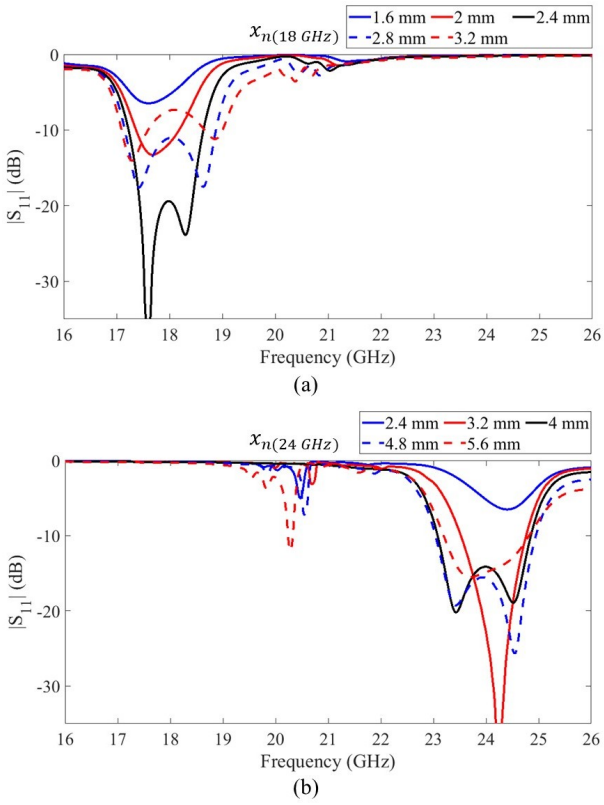

Fig. 4. Simulated $|S_{11}|$ responses of individual radiators for different values of (a) $x_{n(18\ GHz)}$, and (b) $x_{n(24\ GHz)}$

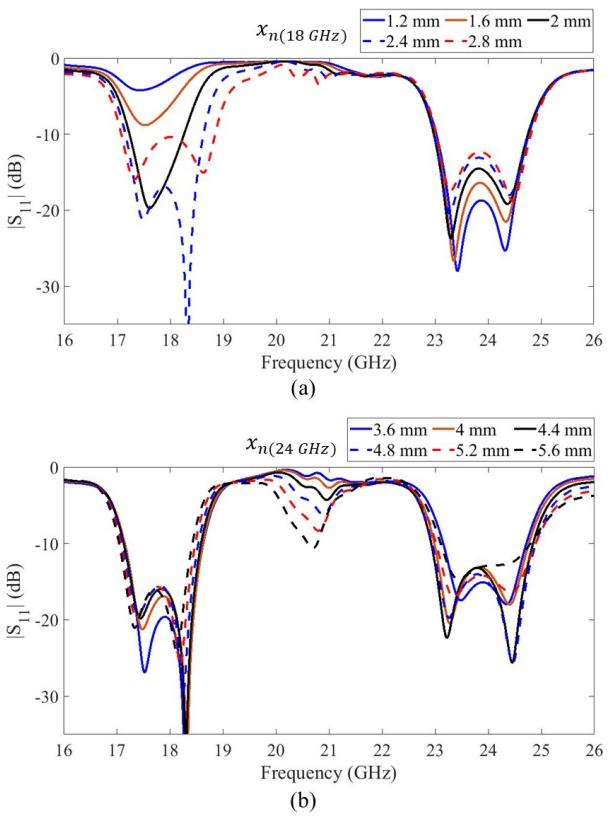

Fig. 5. Simulated $|S_{11}|$ responses of the proposed antenna for different values of (a) $x_{n(18\ GHz)}$, and (b) $x_{n(24\ GHz)}$

The variation in the normalized slot conductance for 18 GHz and 24 GHz slots are plotted in Fig. 3(b) to understand the impedance behaviour of the slots with frequency. It can be observed that the slots for 18 GHz have a significantly low value of G_n at 24 GHz and those for 24 GHz are significantly high at 18 GHz. Hence, the antenna impedance for a certain set of slots causes matching only at the corresponding band while affecting the input impedance and seizing the radiation in the other band. Therefore, the slots for different frequencies can radiate the desired bands despite being placed in proximity of each other while sharing the same antenna aperture. This facilitates the design of the proposed compact dual-band SWA antenna using a single waveguide.

C. Numerical Analysis

The circuit model analysis explained the basic working of the SWA antenna without considering the mutual coupling between the slots which may alter the theoretically optimized values. Therefore, an accurate prediction of the antenna response is carried out by numerically analyzing the antenna using full-wave simulation in CST Studio Suite 2022 in the transient domain solver. The antenna is optimized for individual bands before proceeding to the dual-band design.

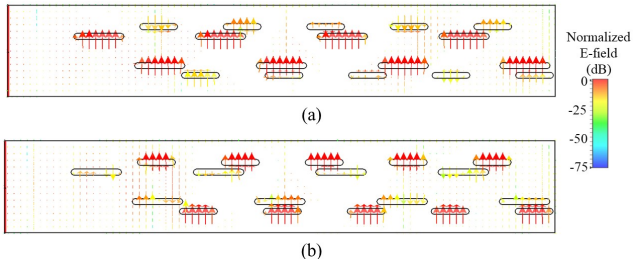

Fig. 6. Simulated E-field vectors across the slots at (a) 18 GHz, and (b) 24 GHz

1) Single Band Design: The waveguide of dimensions a = 15 mm and b = 4.318 mm are used to design single band radiators for 18 GHz and 24 GHz by varying the slot-offset from the waveguide axis. The simulated results for the 18 GHz SWA antenna are summarised in Fig.4(a). It can be observed that the impedance matching can be significantly varied at 18 GHz for different values of $x_{n(18\ GHz)}$ and $|S_{11}| < -10$ dB is achieved for an offset between 2 mm to 3.2 mm. But the best matching response is achieved with $x_{n(18\ GHz)}$ = 2.4 mm which is close to the theoretical estimation, as presented in the previous subsection. In addition, no impedance matching is observed at 24 GHz, which indicates

the isolation of those slots with standing waves of 18 GHz.

The simulated responses of the SWA antenna designed for 24 GHz are shown in Fig. 4(b). It can be observed that $|S_{11}| < -10$ dB can be achieved for $x_{n(24\ GHz)}$ values between 3.2 mm to 5.6 mm where the maximum bandwidth is achieved with $x_{n(24\ GHz)}$ = 4 mm. No impedance matching at the lower frequency band indicates the isolation of the 18 GHz slots with the 24 GHz waveguide field. The point worth mentioning is that the matching response at 24 GHz varies slowly with the slot offset compared to that of the 18 GHz antenna. This is due to the slow variation of G_n with x_n at the higher band as indicated earlier in Fig. 3(b). A weak resonant behaviour is also observed around 20 GHz where the slots are excited with an odd mode which causes a split radiation pattern about the boresight. Since this frequency is outside our frequency of interest, further explanations of this behaviour are beyond the scope of this manuscript.

2) Proposed Dual Band Design: The slots for both frequency bands are placed on the waveguide and simulations are carried out to finalize the dual-band radiator. $x_{n(18\ GHz)}$ and $x_{n(24\ GHz)}$ are individually varied to optimize the geometry by considering their combined effects. The $x_{n(18\ GHz)}$ affects the antenna response significantly around 18 GHz while causing marginal variation in the 24 GHz band as shown in Fig. 5(a). Similar observation can be made from the simulations in Fig. 5(b) where the effects of $x_{n(24\ GHz)}$ are dominantly observed at 24 GHz with insignificant variation in the lower band responses. Therefore, the variation in the antenna response for the corresponding slots is similar to those of the single-band antennas. Moreover the cross-coupling of one set of slots with the performance of the other set may not significantly deteriorate the overall antenna performance. This may ensure sufficient isolation between the slot sets required to operate a single-antenna dual-band system efficiently. Based on the simulation $x_{n(18\ GHz)}$ = 2.4 mm and $x_{n(24\ GHz)}$ = 4 mm are considered optimum for the design of the proposed dual-band SWA antenna.

The E-field vectors across the radiating slots of the proposed antenna are shown in Fig. 6. The 18 GHz fields dominate the corresponding radiating slots where all slots are excited in the same phase as shown in Fig. 6(a). A similar observation can be made with the 24 GHz slots as shown in Fig. 6(b). The cross-coupling of slots with the out-of-band fields can also be observed in both bands which may have a detrimental effect on the antenna performance as mentioned earlier. The total efficiency of approximately 97.7% and 94.5% are recorded at 18 GHz and 24 GHz in simulation.

III. Fabrication and Measurement

The optimized dual-band antenna is fabricated to validate its performance with experimental results.

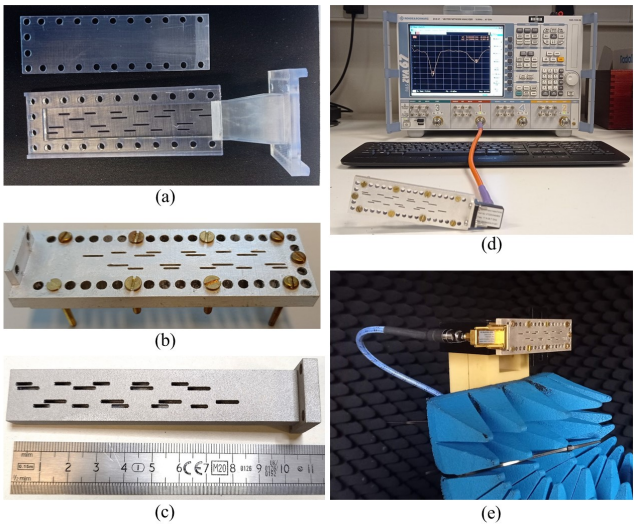

Fig. 7. Fabricated prototype, with SLA 3D printing (a) before metallization, (b) after metallization, and (c) with DMLS 3D printing. Measurement arrangement (d) with VNA during the $|S_{11}|$ measurement, (e) inside an anechoic chamber for radiation pattern measurement.

A. Fabrication

The antenna is fabricated using two different additive manufacturing techniques, namely stereolithography (SLA) and direct metal laser sintering (DMLS) and their measured performances are studied. The adaptation of these 3D printing facilitated immense flexibility in selecting the waveguide dimensions during the design. In a cost-effective SLA technique, a dielectric resin is illuminated with laser which hardens the liquid and forms a solid three-dimensional structure with precision. A Formlabs SLA 3D printer is employed in this process. The fabricated structure has an excellent surface smoothness, robustness and lightweight profile as shown in Fig. 7(a). A transition section is also appended to the dual-band geometry to feed the antenna using a WR-42 waveguide feed. However, the printed structure is dielectric and is metallized to construct the metallic walls of the waveguide. The surfaces of the plastic structure are covered with silver ink using a paintbrush and kept inside an oven at 60^0C for 30 minutes to sinter the paint to form a metallic layer. The structure is fabricated in two sections to facilitate the metallization inside the waveguide walls which are assembled using metallic screws to construct the antenna as shown in Fig. 7(b). The fabrication procedure is fast and cost-effective compared to a commercial DMLS technique. In addition, the prototype has a smooth surface and is lighter than a conventional metal-milled product.

The same in DMLS is constructed in a single piece by illuminating metal powder layers with high-power laser beams. The single-unit structure avoids the multi-part assembly with screws and has an accurate geometry with good surface smoothness, mechanical robustness and lightweight. The pro-

This article has been accepted for publication in IEEE Transactions on Antennas and Propagation. This is the author's version which has not been fully edited and content may change prior to final publication. Citation information: DOI 10.1109/TAP.2024.3484150

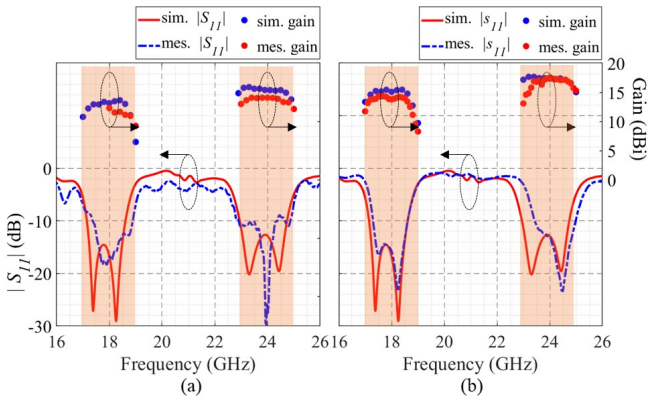

Fig. 8. Simulated and measured $|S_{11}|$ and gain of the fabricated prototype with (a) SLA and (b) DMLS. The simulated structures are identical to the corresponding fabricated prototypes.

totype also consists of a transition and WR-42 flange and has a narrow width due to the absence of the supporting screw holes as shown in Fig. 7(c). Therefore a compact antenna array with a better side lobe response may be constructed in the DMLS technique. In addition, the all-metal structure may offer a better gain due to low loss. However, the fabrication process is costly and requires more time and expertise in handling the overall machinery.

B. Measurement

The fabricated prototypes are tested to characterize the dual-band antenna response. A four-channel Rohde & Schwarz ZVA 67 vector network analyzer (VNA) operating from 10 MHz to 67 GHz has been employed to measure the input impedance of the antenna. A photograph of the measurement arrangement of the antenna with VNA is shown in Fig. 7(d). The VNA is SOLT (short-open-load-through) calibrated over 16-26 GHz using a conventional WR-42 waveguide calibration kit to shift the reference plane at the antenna input. A Vector Telecom Pty Ltd waveguide to the coaxial adapter is used to excite the antenna using a co-axial feed.

The simulated and measured $|S_{11}|$ of the fabricated prototype with SLA are shown in Fig. 8(a). Good impedance matching is measured at 18 GHz and 24 GHz as $|S_{11}| < -10$ dB are observed at these frequencies in both fabrication techniques. The measured results also meet the typical space-qualified impedance matching criteria of -15 dB at these frequencies. A -10 dB impedance bandwidth of approximately 1.5 GHz is measured in both bands. In addition, the measured result matches well with the simulated estimation which validates the accuracy of the numerical estimation. Similar observations can be made with the simulated and measured results with DMLS as shown in Fig. 8(b). A smoother measured data with DMLS indicates a uniformly fabricated geometry with reduced internal reflections inside the structure.

Following the measurement of the impedance matching of the antenna, its gain is measured from the measurement of radiation patterns. The radiation pattern is measured inside an anechoic chamber compatible to perform measurements up to 67 GHz. The antenna is placed at the receiving side of the chamber above a rotating platform to enable an antenna rotation on its E- and H-planes. It is irradiated using a wideband horn antenna at the transmitting end of the chamber which is also attached to a rotating platform to enable the co- and cross-polar measurements. An A-INFO horn antenna having a 3.5 mm female coaxial input is used to transmit linearly polarised plane waves over 18 GHz to 26.5 GHz [18]. The maximum antenna gain is measured from the co-polarised data with the SLA and DMLS prototypes as plotted against the simulated estimations in Fig. 8. Absolute gains of 12.4 dBi and 14.3 dBi are measured against the simulated gains of 14.2 dBi and 15.7 dBi gains at 18 GHz and 24 GHz with the SLA prototype as shown in Fig. 8(a). The same with DMLS are 14 dBi and 17.6 dBi against the simulated gains of 15 dBi and 17.4 dBi at 18 GHz and 24 GHz, respectively. The measured data in the former process suffers from a consistent deviation from the simulated results, possibly due to the losses in the fabricated geometry. These losses may be due to the host dielectric material and hand-made metal painting which may be the bottleneck of the SLA-based fabrication approach. On the other hand, those with the DMLS technique match well with simulation which may be due to the geometric accuracy and for the all-metal implementation. Other discrepancies in the measured results may be due to the mismatch of the phase centres of the transmitting and receiving antenna during the measurement where the antenna locations were manually adjusted to ensure a boresight-to-boresight alignment between the radiators. There may be additional losses due to an imperfect fabrication of the flange region where small geometric deviation may cause observable effects in the measured results. The geometric deviation may be during the cooling down phase following the laser heating where structural bending may happen due to a nonuniform heat dissipation.

The simulated and measured E- and H-plane radiation patterns at 18 GHz and 24 GHz are shown for the SLA and DMLS in Fig. 9(a) and (b), respectively. It can be observed that the radiation is unidirectional and in the boresight of the antenna. The side lobe levels are approximately 10 dB below the boresight gains in all planes. The cross-polar patterns are significantly less than those of the co-pole indicating the polarisation purity of the linearly polarised antenna. The E-plane patterns are wider than those of the H-plane due to the distribution of the slot array on the latter plane. The measured results match well with the numerical analysis with small discrepancies. The boresight gain drop at 18 GHz on

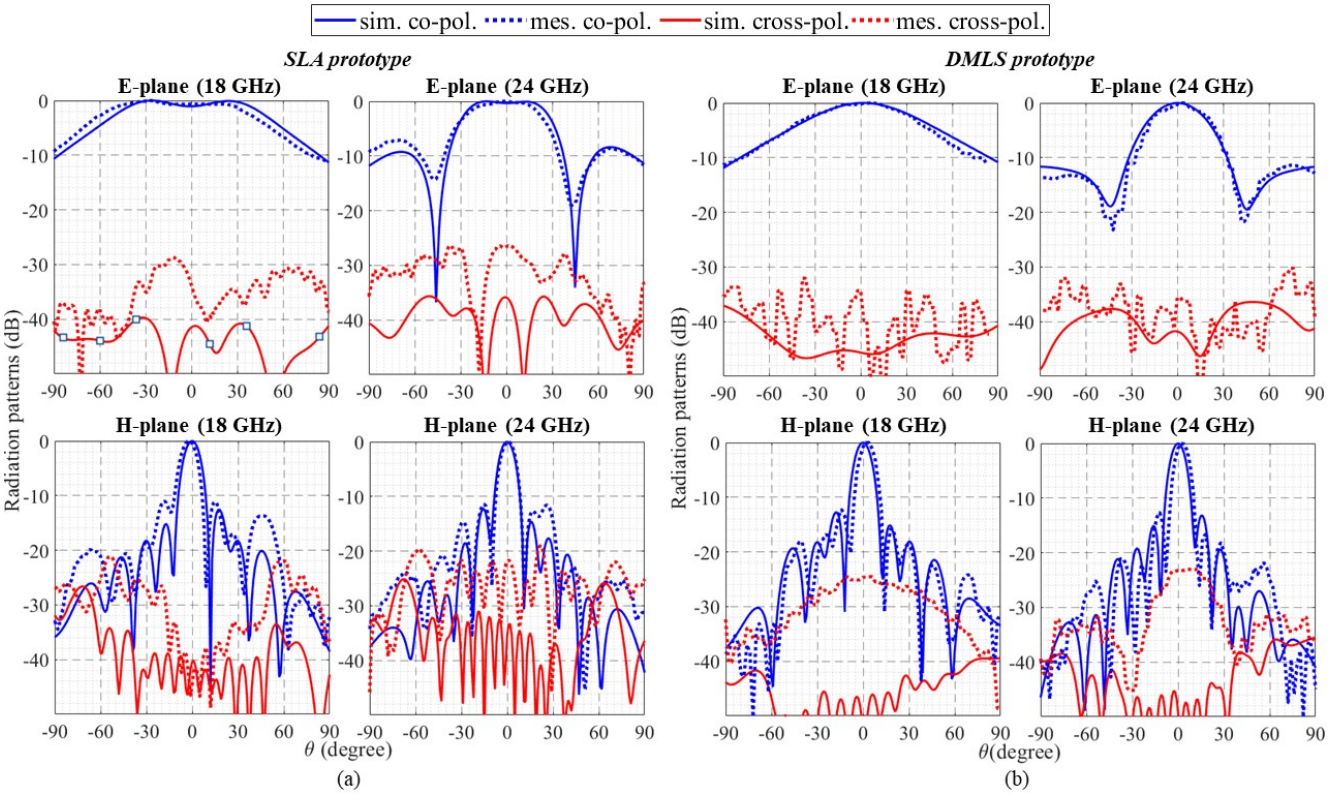

Fig. 9. Simulated and measured radiation patterns on the E-plane and H-plane of the antenna at 18 GHz and 24 GHz with (a) SLA and (b) DMLS techniques. The simulated structures are the exact geometries used for printing.

TABLE I
COMPARISON OF THE STATE OF THE ART SOLUTIONS OF DUAL-BAND SWA ANTENNAS

Ref.	$\{f_{min}, f_{max}\}$ (GHz)	Aperture area**	Gains at $\{f_{min}, f_{max}\}$ (dBi)	Feeding technique	Single polarisation	Unidirectional radiation pattern	Single waveguide #
[8]	{30, 35}	10λ×7.6λ	{25.4, 24.8}	coupling slot	no	yes	no
[9]	{1.25, 5.4}	13.2λ×2.4λ	{25.9, 26.1}	multiple probes	no	yes	no
[10]	{10, 15.2}	7.4λ×2.3λ	{14.3, 17.4}	two probes	yes	yes	no
[11]	{2.5, 4.9}	12.3λ×1.3λ	{11.1, 18.9}	single probes	no	no	yes
[12]	{2.25, 4.9}	13.8λ×1.3λ	{14.4, 17.6}	single probes	no	no	yes
[13]	{9.4, 32}	32.6λ×2.4λ	××	two probes	yes	yes	no
[14]	{18, 24}	10.1λ×1.7λ	{14.6, 15.9}	waveguide flange	yes	yes	no
[15]	{10, 15}	14.7λ×1.4λ	{14.9, 19.3}	waveguide flange	yes	yes	no
Proposed	{18, 24}	6.5λ×1.4λ	{14, 17.6}	waveguide flange	yes	yes	yes

** λ refers to free space wavelength of the highest operating frequency
# refers to the radiating waveguide element/elements responsible for dual-band radiation

the E-plane of the SLA prototype is due to the propagation of surface waves on the extended metallic region for the screw holes. This region makes the antenna width approximately double of the free space wavelength at 18 GHz which can support more than one wavefront from the total aperture and reduces the antenna gain in boresight. The same can also be observed from the E-plane pattern at 24 GHz. The E-plane nulls at 24 GHz are due to the total gap between the corresponding slots which is more than $\lambda_{24GHz}/2$ where, λ_{24GHz} is the free space wavelength at 24 GHz, as observed in the SLA and DMLS prototypes.

A quantitative comparison among the state-of-the-art solutions of dual-band SWA antennas is presented in Table.I. The proposed technique implements one of the most compact dual-band SWA antennas radiating a single polarisation in one direction while fed through a simple waveguide flange at its input. This excitation technique does not require any additional matching network, nor does its placement depend on the operating frequency which makes the feeding network simple for a waveguide-based dual-band geometry. Moreover,

the use of a single waveguide for two frequency bands makes this design simple, compact and unique, by considering the radiation direction and the dual-band polarisation of the antenna, simultaneously.

IV. Conclusion

This article presents the design of a compact slotted waveguide array (SWA) antenna for dual-band applications by placing the longitudinal slots of both frequencies on the same broad wall of a waveguide. The design is intended for 18 GHz and 24 GHz of the $K-$band applications. Its working is theoretically explained with a circuit model to discuss the interdependence of antenna dimensions with the slot excitation coefficients and the input impedance. The antenna width is optimised to avoid the overlap of the radiating slots for a desired antenna response. Following the theoretical discussion, numerical analyses are carried out to incorporate the mutual coupling among the slots through full-wave simulations. It is numerically shown that the antenna optimised for individual bands can be placed together to implement the dual-band geometry. The numerically optimised structure is fabricated using stereolithography (SLA) and direct metal laser sintering (DMLS) additive manufacturing techniques. It enabled significant flexibility in the design in addition to construct a robust and lightweight prototype. The fabricated prototype is characterised by measuring its input impedance where, $|S_{11}| < -10$ dB are observed at 18 GHz and 24 GHz with approximately 1.5 GHz of impedance bandwidths. Boresight antenna gains of14 dBi and 17.4 dBi are measured with the all-metal DMLS-based prototype from the unidirectional radiation patterns of linear polarisation. A comparative study between the antenna performances of SLA and DMLS techniques and those with state-of-the-art solutions is also discussed. In summary, the working of a compact dual-band antenna with an all-metal geometry is explained with theoretical, numerical and experimental results to propose a new approach of multi-band antenna design by placing the radiating elements on a common antenna aperture while exciting a single waveguide.

V. Acknowledgment

The authors thank Thales for their assistance and funding.

References

[1] R. Elliott and L. Kurtz, "The Design of Small Slot Arrays," *IEEE Tran. Antennas Propag.*, vol. 26, no. 2, pp. 214-219, March 1978.

[2] N. Bartolomei, D. Blanco, F. Doucet, Etienne Girard, H. Legay *et al.*, "A Circularly Polarized Parallel Plate Waveguide Lens-Like Multiple-Beam Linear Array Antenna for Satcom Applications," *IEEE Access*, vol. 11, pp. 4602-4614, 2023.

[3] A. F. Stevenson, "Theory of Slots in Rectangular Wave-Guides," *J Appl. Phys.* 19, pp. 24–38, 1948.

[4] R. Elliott, "An Improved Design Procedure for Small Arrays of Shunt Slots," *IEEE Tran. Antennas Propag.*, vol. 31, no. 1, pp. 48-53, January 1983.

[5] L. Ripoll-Solano, L. Torres-Herrera and M. Sierra-Pérez, "Design, Simulation and Optimization of a Slotted Waveguide Array with Central Feed and Low Sidelobes," *2018 IEEE-APS Topical Conference on Antennas and Propagation in Wireless Communications (APWC)*, Cartagena, Colombia, 2018, pp. 886-889.

[6] R. J. Stegen, "Slot radiators and arrays at X-band," *Tran. IRE Professional Group Antennas Propag.*, vol. 1, no. 1, pp. 62-84, Feb. 1952.

[7] L. A. Ripoll Solano, M. Sierra Perez and D. Pardo Santos, "Design, Simulation and Test of a Slot Antenna Array using one Parameter Taylor Synthesis in the GHz Range," *IEEE Latin America Tran.*, vol. 13, no. 10, pp. 3210-3215, Oct. 2015.

[8] T. Li, H. Meng and W. Dou, "Design and Implementation of Dual-Frequency Dual-Polarization Slotted Waveguide Antenna Array for Ka-Band Application," *IEEE Antennas Wireless Propag. Lett.*, vol. 13, pp. 1317-1320, 2014.

[9] M. Chen, X. -C. Fang, W. Wang, H. -T. Zhang and G. -L. Huang, "Dual-Band Dual-Polarized Waveguide Slot Antenna for SAR Applications," *IEEE Antennas Wireless Propag. Lett.*, vol. 19, no. 10, pp. 1719-1723, Oct. 2020.

[10] D. -J. Wei, J. Li, G. Yang, J. Liu and J. -J. Yang, "Design of Compact Dual-Band SIW Slotted Array Antenna," *IEEE Antennas Wireless Propag. Lett.*, vol. 17, no. 6, pp. 1085-1089, June 2018.

[11] C. S. Arismar, I. F. da Costa, S. Pinna, S. Melo, F. Laghezza et al., "A novel dual-polarization and dual-band slotted waveguide antenna array for dual-use radars," *2016 10th European Conference on Antennas and Propagation (EuCAP)*, Davos, Switzerland, 2016, pp. 1-4.

[12] I. F. da Costa, R. A. Santos, S. C. Patricio, J. A. J. Ribeiro, D. H. Spadoti et al., "A dual-band slotted waveguide antenna array for radars applications," *2015 SBMO/IEEE MTT-S International Microwave and Optoelectronics Conference (IMOC), Porto de Galinhas, Brazil, 2015*, pp. 1-4.

[13] M. Khorramizadeh, A. R. Mallahzadeh, R. Jesri, S. M-A-Nezhad, "Dual-Band Ridged Tapered Waveguide Slot Array Antenna With Cross-Polarisation Reduction," *IET Microw. Antennas Propag.*, vol. 12, issue 14, pp. 2255-2261, Nov. 2018.

[14] A. Roy, R. Allanic, T. L. Gouguec, E. Fourn, A. -C. Amiaud and H. Legay, "A Dual-Band Single-Feed SWA by Cascading Waveguides for Unidirectional Radiation Patterns," *2023 IEEE Conference on Antenna Measurements and Applications (CAMA)*, Genoa, Italy, 2023, pp. 578-581.

[15] A. Roy, R. Allanic, T. L. Gouguec, E. Fourn, A. -C. Amiaud and H. Legay,"Conception d'une Antenne Guide à Fentes Bi-Fréquences Optimisée pour la Mise en Réseau,"*accepted in XXIIIèmes Journées Nationales Microondes*, 2024.

[16] G. P. Le Sage, "3D Printed Waveguide Slot Array Antennas," *IEEE Access*, vol. 4, pp. 1258-1265, 2016.

[17] A. Roy, "Matlab Code to Design A Slotted Waveguide Array Antenna," *ResearchGate*, Jan. 2024, [Online], Available: https://www.researchgate.net/publication/377407283_Matlab_Code_to_Design_A_Slotted_Waveguide_Array_Antenna.

[18] A-INFO, "LB-42-10-C-3.5F Datasheet," [Online], Available: https://www.ainfoinc.com/lb-42-10-c-3-5f-standard-gain-horn-antenna-18-26-5-ghz-10db-gain-3-5mm-female.